Optical Signal Processing for W-Band Radio-Over-Fiber System With Tunable Frequency Response

Run-Kai Shiu, You-Wei Chen, Peng-Chun Peng, Ming-Han Wen, Shang-Jen Su, Chin-Wei Hsu, and Gee-Kung Chang, *Fellow, IEEE*

***Abstract*—Tunable frequency response is designed and experimentally demonstrated in this paper. The performance of frequency response in proposed radio-over-fiber (RoF) systems is investigated in terms of theoretical analysis, simulations, and experimental results with various fiber transmission distances. The notch in frequency response can be easily circumvented by changing the oriented angle of polarized lightwave in the proposed direct detection (DD) scheme. For comparison, the conventional Mach-Zehnder modulator (MZM) based DD scheme suffers from fixed frequency notch at certain frequencies, which generates forbidden frequency bands for W-band signal delivery. Our experimental results show that the proposed DD scheme exhibits a stable EVM performance of the 16-QAM signal from 83 GHz to 87 GHz via 25-km standard single-mode fiber (SSMF) and 1-m wireless transmission. On the contrary, the conventional MZM-based DD scheme encounters severe signal degradation at 85 GHz and 86 GHz. In this paper, the proposed scheme is implemented to demonstrate full bandwidth availability within a desirable frequency range by tuning the frequency response. Furthermore, a 10-Gbps 16-QAM signal located at 85 GHz is successfully transmitted by the proposed DD scheme which can provide 10-gigabit data transmission under 5G requirement.**

***Index Terms*—Optical signal processing, radio-over-fiber, W-band.**

I. Introduction

RECENTLY, the demand for high-quality media applications such as virtual reality (VR), augmented reality (AR) and 8K video streaming is increasing in mobile data communications. However, the conventional wireless spectra of below 6 GHz are already heavily congested which is very challenging to provide multi-gigabit data transmission with limited frequency resource. Therefore, the urgency to deploy millimeter-wave (MMW) frequency bands with large bandwidth has been investigated by the telecommunication community [1]–[8]. W-band (75–110 GHz) signals exhibiting lower air absorption loss than V-band (45–75 GHz), would be a valuable radio frequency (RF) band to address the issue on bandwidth shortage. To generate and transmit such high-frequency signals, radio-over-fiber (RoF) system with photonic-aided techniques have been developed [9]–[16]. In these reports, a simple remote radio unit (RRU) design and centralized management with low-latency data transmission, has been investigated. Intensity-modulation and direct detection (IM-DD) system has simple hardware design at the RRU side, and MMW signals can be generated by the heterodyne beaten optical sidebands after square law detection thorough the photodetector (PD) [17], [18]. Since the optical sidebands are generated by the Mach-Zehnder modulator (MZM) driven by RF input signals, the generated MMW signal in the distributed unit (DU) is more stable than those signals generated by using two free-running lasers without frequency locking [19]. However, the RF selective power fading caused by the chromatic dispersion in fiber transmission depending on fiber length and employed RF frequency, may cause severe signal degradation at certain frequencies. Moreover, this frequency fading is getting worse for the very high-frequency signal (i.e. W-band signal) through a 25-km standard single-mode fiber (SSMF) in the mobile fronthaul. Thus, it leads to forbidden frequencies located in the W-band that wastes valuable frequency resources. To mitigate the chromatic dispersion induced RF power fading effect in W-band, the optical single sideband (OSSB) modulation based on optical filtering is proposed [20]. However, strictly designed optical filters should be utilized and it is also susceptible to the bandwidth of the modulated signal. Other methods to address this impairment in different frequency bands such as separate modulation and combination of the sidebands, using silicon ring-modulations, and transmitting duplicated data streams on two wavelength channels via two opposite-chirped modulators have been investigated [21]–[23]. Comparing to MZM, polarization modulator (PolM), which is immune from

Manuscript received May 25, 2020; revised July 5, 2020; accepted July 26, 2020. Date of publication July 30, 2020; date of current version August 28, 2020. This paper was supported by the Ministry of Science and Technology, Taiwan, under Grants MOST 108-2221-E-027 -040 -MY2 and MOST 108-2917-I-027 -001. *(Corresponding author: Peng-Chun Peng.)*

Run-Kai Shiu is with the Department of Electro-Optical Engineering, National Taipei University of Technology, Taipei 10608, Taiwan, and also with the School of Electrical and Computer Engineering, Georgia Institute of Technology, Atlanta, GA 30308 USA (e-mail: t106659002@ntut.edu.tw).

You-Wei Chen, Shang-Jen Su, Chin-Wei Hsu, and Gee-Kung Chang are with the School of Electrical and Computer Engineering, Georgia Institute of Technology, Atlanta, GA 30308 USA (e-mail: yu-wei.chen@ece.gatech.edu; taiwanjen@gatech.edu; chsu95@gatech.edu; gkchang@ece.gatech.edu).

Peng-Chun Peng and Ming-Han Wen are with the Department of Electro-Optical Engineering, National Taipei University of Technology, Taipei 10608, Taiwan (e-mail: pcpeng@ntut.edu.tw; t108658005@ntut.edu.tw).

Color versions of one or more of the figures in this article are available online at https://ieeexplore.ieee.org.

Digital Object Identifier 10.1109/JSTQE.2020.3012598

1077-260X © 2020 IEEE. Personal use is permitted, but republication/redistribution requires IEEE permission.
See https://www.ieee.org/publications/rights/index.html for more information.

Authorized licensed use limited to: Georgia Institute of Technology. Downloaded on July 08,2021 at 19:08:57 UTC from IEEE Xplore. Restrictions apply.

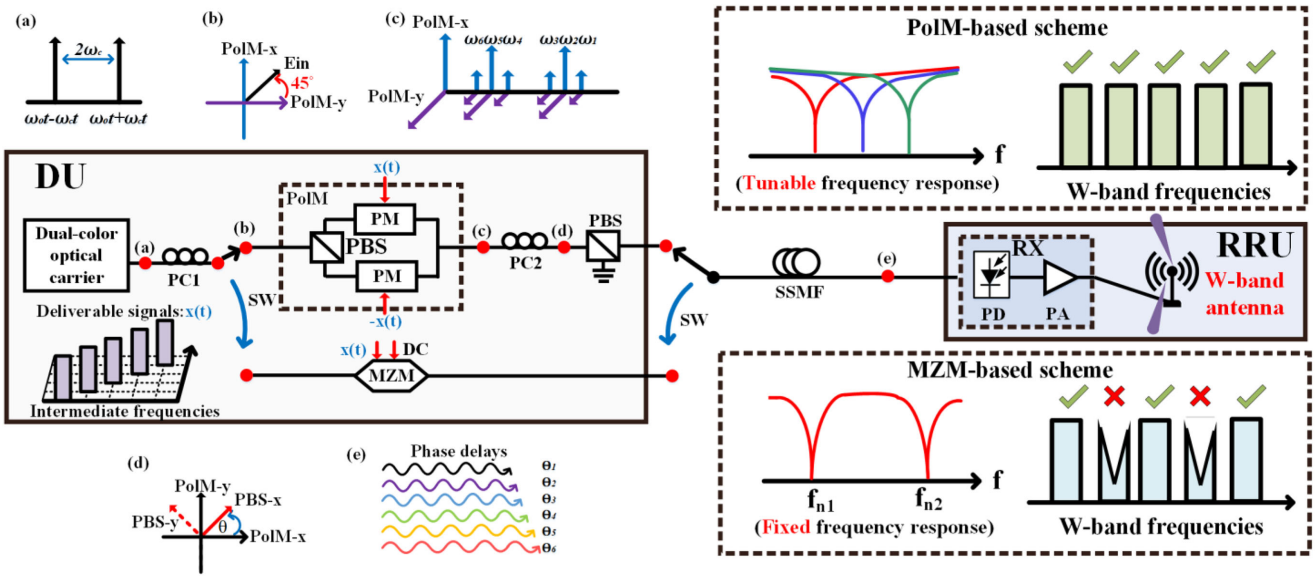

Fig. 1. Schematic diagram of the proposed PolM-based and the conventional MZM-based DD schemes. (DU: distributed unit, PC: polarization controller, SW: switch, PolM: polarization modulator, PM: phase modulator, MZM: Mach-Zehnder modulator, PBS: polarization beam splitter, SSMF: standard single-mode fiber, RRU: remote radio unit, RX: receiver, PD: photodetector, PA: power amplifier.)

DC drifting problem, is an alternative that can be applied in the DD system. PolM is a special phase modulator that can support both transverse-electric (TE) and transverse-magnetic (TM) modes with opposite phase modulation indices [24]. A DD system based on PolM was successfully implemented to enhance the signal bandwidth of PAM-4 signal transmission [25]. Additionally, a photonic microwave notch filter based on a PolM was also achieved and demonstrated at 27-GHz and 28-GHz by shifting the frequency notch to remove the unwanted signal [26]. In our previous work, the PolM-based structure was proposed to shift the frequency notches in W-band to make sure the transmitted MMW signals can survive from RF fading effect [27] where only QPSK modulation format was applied in a proof of concept experiment without detailed theoretical analysis.

In this paper, we propose and demonstrate a DD RoF system with tunable frequency response using a dual-color optical carrier source and a PolM. The dual-color optical carrier source is employed to generate an optical MMW signal with adjustable wavelength spacing. The frequency responses of both proposed PolM-based and conventional MZM-based DD schemes are simulated and analyzed. Moreover, the multi-tone signals are used to modulate the dual-color optical carrier to investigate the frequency response after fiber transmission. System simulations are conducted to verify the theoretical analysis and experimental results of the tunable frequency response. For W-band RoF transport system, 1Gbaud 16-QAM signals carried by different intermediate frequencies (IF) from 3 GHz to 7 GHz are inserted into the PolM and MZM to modulate the dual-color optical carrier, respectively. In the proposed scheme, we can easily manage the frequency notch due to RF power fading by rotating the polarization controller (PC) to vary the angle between the polarized lightwave and the subsequent polarizer. Therefore, the desired W-band signals can be arbitrarily assigned to fully explore the available bands. Comparing with conventional MZM-based DD scheme which encounters forbidden transmission bands, the proposed scheme can efficiently use the full bandwidth in W-band by the optical signal processing via tuning frequency response. The rest of the paper is organized as follows: Section II. describes the theoretical analysis of frequency response of the proposed PolM-based and conventional MZM-based DD schemes; Section III. exhibits the experimental setup and results as well as simulations of the investigation on the frequency response; Section IV. presents experimental setup and results of the W-band RoF transport system based on the proposed PolM-based DD scheme and the conventional MZM-based DD schemes; Section V. depicts the conclusion of the presented work.

II. Theoretical Analysis

Schematic diagrams of the conventional MZM-based and proposed PolM-based DD system are shown in the Fig. 1. In the DU, the dual-color optical carrier with adjustable wavelength spacing is modulated by the IF band signals to up-convert the IF signal to higher desired frequency band (i.e.W-band) by heterodyne beating through the PD at the RRU. Whereas, if the IF signal is modulated by the MZM, the periodically frequency notches at fn1 and fn2 caused by the chromatic dispersion will deteriorate the signals at these frequencies resulting the forbidden bands for data delivery. This will reduce the flexibility of the network. On the contrary, the frequency notch can be shifted by changing the lightwave incident angle to the polarizer in the proposed PolM-based scheme. With the capability of tuning the frequency response, the desired W-band signal can always survive from the RF frequency notch in any IF arrangement. The detailed theoretical analysis is elaborated below. To generate the dual-color optical carrier, the tunable laser source with amplitude and angular frequency of E_0 and ω_0 is modulated via a sinusoid RF

Authorized licensed use limited to: Georgia Institute of Technology. Downloaded on July 08,2021 at 19:08:57 UTC from IEEE Xplore. Restrictions apply.

signal with angular frequency of ω_c by a MZM. To suppress the carrier, the MZM is biased at null point and thus the output E-filed of MZM can be expressed as

$$\begin{aligned} E_{MZM-out} &= \frac{1}{2}\mathrm{E}_0 e^{j(\omega_0 t)}(e^{jm_1\cos(\omega_c t)}e^{j\frac{\pi}{2}} \\ &\quad + e^{j(-m_1\cos(\omega_c t))}e^{-j\frac{\pi}{2}}) \\ &= \frac{1}{2}\mathrm{E}_0 e^{j(\omega_0 t)}(\sum_{n=-\infty}^{\infty} j^n J_n(m_1)e^{jn\omega_c t}e^{j\frac{\pi}{2}} \\ &\quad + \sum_{n=-\infty}^{\infty} j^n J_n(m_1)e^{jn(\omega_c t+\pi)}e^{-j\frac{\pi}{2}}) \end{aligned} \quad (1)$$

where m_1 is the modulation index of the MZM, J_n is the first kind Bessel function of the n[th] term. By neglecting the higher order terms (n>1) for simplicity, we have

$$\begin{aligned} E_{MZM-out} &= -\mathrm{E}_0 J_1(m_1)e^{j(\omega_0 t-\omega_c t)} \\ &\quad + \mathrm{E}_0 J_1(m_1)e^{j(\omega_0 t+\omega_c t+\pi)} \\ &= -\mathrm{E}_1 e^{j(\omega_0 t-\omega_c t)} + \mathrm{E}_1 e^{j(\omega_0 t+\omega_c t+\pi)} \end{aligned} \quad (2)$$

Eq. (2) exhibits the E-filed of the dual-color optical carrier of which the schematic optical spectrum is shown in Fig. 1(a). In the proposed PolM-based DD scheme, the dual-color optical carrier is connected to the PC1 prior to the PolM to align the lightwave to 45 degrees with respect to the x-axis of PolM as shown in Fig. 1(b). Thus, the lightwave is equally projected to both axes of PolM and modulated by another RF signal with angular frequency of ω_r. Inset (c) of Fig. (1) illustrates the output E-field of PolM which is

$$\begin{bmatrix} E_{PolM-x} \\ E_{PolM-y} \end{bmatrix} = \frac{1}{\sqrt{2}}\mathrm{E}_1 \begin{bmatrix} (-e^{j(\omega_0 t-\omega_c t)} + e^{j(\omega_0 t+\omega_c t+\pi)}) \\ \times e^{j(m_2\cos(\omega_r t))} \\ (-e^{j(\omega_0 t-\omega_c t+\phi)} + e^{j(\omega_0 t+\omega_c t+\pi+\phi)}) \\ \times e^{j(-m_2\cos(\omega_r t))} \end{bmatrix} \quad (3)$$

where m_2 is the modulation index of PolM and ϕ is the phase difference between x- and y-axis of PolM which can also be adjusted by PC1. By applying Jacobi-anger expansion to (3), we have

$$\begin{bmatrix} E_{PolM-x} \\ E_{PolM-y} \end{bmatrix} = \frac{1}{\sqrt{2}}\mathrm{E}_1 e^{j\omega_0 t} \begin{bmatrix} +J_1(m_2)\mathrm{e}^{j(\omega_c t+\omega_r t+\frac{3\pi}{2})} \\ +J_0(m_2)\mathrm{e}^{j(\omega_c t+\pi)} \\ -J_1(m_2)\mathrm{e}^{j(\omega_c t-\omega_r t+\frac{\pi}{2})} \\ -J_1(m_2)\mathrm{e}^{j(-\omega_c t+\omega_r t+\frac{\pi}{2})} \\ -J_0(m_2)\mathrm{e}^{j(-\omega_c t)} \\ +J_1(m_2)\mathrm{e}^{j(-\omega_c t-\omega_r t-\frac{\pi}{2})} \\ +J_1(m_2)\mathrm{e}^{j(\omega_c t+\omega_r t+\frac{\pi}{2}+\phi)} \\ +J_0(m_2)\mathrm{e}^{j(\omega_c t+\pi+\phi)} \\ -J_1(m_2)\mathrm{e}^{j(\omega_c t-\omega_r t+\frac{3\pi}{2}+\phi)} \\ -J_1(m_2)\mathrm{e}^{j(-\omega_c t+\omega_r t-\frac{\pi}{2}+\phi)} \\ -J_0(m_2)\mathrm{e}^{j(-\omega_c t+\phi)} \\ +J_1(m_2)\mathrm{e}^{j(-\omega_c t-\omega_r t+\frac{\pi}{2}+\phi)} \end{bmatrix} \quad (4)$$

The PC2 and a polarization beam splitter (PBS) are utilized as a polarizer. The PC2 is employed to orient the angle between the principal axis of PolM and the PBS. For instance, if the x-axis of PolM is oriented at θdegrees to the x-axis of the PBS as shown in Fig. 1(d), the output E-field of x-axis of the PBS is written as

$$[\mathrm{E}_{\mathrm{PBS-x}}] = [\cos\theta \mathrm{E}_x + \sin\theta \mathrm{E}_y] \quad (5)$$

As the SSMF is a dispersive medium, the lightwave with different optical angular frequencies will experience different phase delays after traveling in the fiber. Therefore, we utilize the second order Taylor series to express the phase delay near the optical frequency ω_0 which is

$$\theta(\omega) \approx z\beta(\omega_0) + z\dot{\beta}(\omega_0)(\omega-\omega_0) + \frac{1}{2}z\ddot{\beta}(\omega_0)(\omega-\omega_0)^2 \quad (6)$$

where $\dot{\beta}(\omega_0)$ and $\ddot{\beta}(\omega_0)$ are the first and second derivatives of $\beta(\omega_0)$ in regard to ω_0 and z is the length of SSMF. Eq. (7) and the point (e) of Fig. 1 illustrate the phase delays of six optical components after fiber transmission as

$$\begin{aligned} &\omega_1 = \omega_0 + \omega_\mathrm{c} + \omega_\mathrm{r}, \\ &\theta_1 = \mathrm{z}\beta(\omega_0) + \mathrm{z}\dot{\beta}(\omega_0)(\omega_\mathrm{c}+\omega_\mathrm{r}) + \frac{1}{2}\mathrm{z}\ddot{\beta}(\omega_0)(\omega_\mathrm{c}+\omega_\mathrm{r})^2 \\ &\omega_2 = \omega_0 + \omega_\mathrm{c}, \theta_2 = \mathrm{z}\beta(\omega_0) + \mathrm{z}\dot{\beta}(\omega_0)(\omega_\mathrm{c}) + \frac{1}{2}\mathrm{z}\ddot{\beta}(\omega_0)(\omega_\mathrm{c})^2 \\ &\omega_3 = \omega_0 + \omega_\mathrm{c} - \omega_\mathrm{r}, \\ &\theta_3 = \mathrm{z}\beta(\omega_0) + \mathrm{z}\dot{\beta}(\omega_0)(\omega_\mathrm{c}-\omega_\mathrm{r}) + \frac{1}{2}\mathrm{z}\ddot{\beta}(\omega_0)(\omega_\mathrm{c}-\omega_\mathrm{r})^2 \\ &\omega_4 = \omega_0 - \omega_\mathrm{c} + \omega_\mathrm{r}, \\ &\theta_4 = \mathrm{z}\beta(\omega_0) + \mathrm{z}\dot{\beta}(\omega_0)(-\omega_\mathrm{c}+\omega_\mathrm{r}) + \frac{1}{2}\mathrm{z}\ddot{\beta}(\omega_0)(-\omega_\mathrm{c}+\omega_\mathrm{r})^2 \\ &\omega_5 = \omega_0 - \omega_\mathrm{c}, \theta_5 = \mathrm{z}\beta(\omega_0) + \mathrm{z}\dot{\beta}(\omega_0)(-\omega_\mathrm{c}) + \frac{1}{2}\mathrm{z}\ddot{\beta}(\omega_0)(-\omega_\mathrm{c})^2 \\ &\omega_6 = \omega_0 - \omega_\mathrm{c} - \omega_\mathrm{r}, \\ &\theta_6 = \mathrm{z}\beta(\omega_0) + \mathrm{z}\dot{\beta}(\omega_0)(-\omega_\mathrm{c}-\omega_\mathrm{r}) + \frac{1}{2}\mathrm{z}\ddot{\beta}(\omega_0)(-\omega_\mathrm{c}-\omega_\mathrm{r})^2 \end{aligned} \quad (7)$$

By introducing the phase delays to their corresponding optical terms, the optical components received at PD can be written as

$$E_{out} = \frac{1}{\sqrt{2}}\mathrm{E}_1 e^{j\omega_0 t}\left\{ \cos\theta \begin{bmatrix} +J_1(m_2)\mathrm{e}^{j(\omega_c t+\omega_r t+\frac{3\pi}{2}+\theta_1)} \\ +J_0(m_2)\mathrm{e}^{j(\omega_c t+\pi+\theta_2)} \\ -J_1(m_2)\mathrm{e}^{j(\omega_c t-\omega_r t+\frac{\pi}{2}+\theta_3)} \\ -J_1(m_2)\mathrm{e}^{j(-\omega_c t+\omega_r t+\frac{\pi}{2}+\theta_4)} \\ -J_0(m_2)\mathrm{e}^{j(-\omega_c t+\theta_5)} \\ +J_1(m_2)\mathrm{e}^{j(-\omega_c t-\omega_r t-\frac{\pi}{2}+\theta_6)} \end{bmatrix} + \sin\theta \begin{bmatrix} +J_1(m_2)\mathrm{e}^{j(\omega_c t+\omega_r t+\frac{\pi}{2}+\phi+\theta_1)} \\ +J_0(m_2)\mathrm{e}^{j(\omega_c t+\pi+\phi+\theta_2)} \\ -J_1(m_2)\mathrm{e}^{j(\omega_c t-\omega_r t+\frac{3\pi}{2}+\phi+\theta_3)} \\ -J_1(m_2)\mathrm{e}^{j(-\omega_c t+\omega_r t-\frac{\pi}{2}+\phi+\theta_4)} \\ -J_0(m_2)\mathrm{e}^{j(-\omega_c t+\phi+\theta_5)} \\ +J_1(m_2)\mathrm{e}^{j(-\omega_c t-\omega_r t+\frac{\pi}{2}+\phi+\theta_6)} \end{bmatrix} \right\} \quad (8)$$

Authorized licensed use limited to: Georgia Institute of Technology. Downloaded on July 08,2021 at 19:08:57 UTC from IEEE Xplore. Restrictions apply.

The photo current detected by the PD only considering frequency terms of $2\omega_c t + \omega_r t$ is

$$i_{PD-PolM} = \frac{1}{2}\mathrm{E}_1 J_0(m_2)J_1(m_2) \times \begin{Bmatrix} -\cos^2\theta e^{j(2\omega_c t+\omega_r t+\frac{3\pi}{2}+\theta_1-\theta_5)} \\ -\cos\theta\sin\theta e^{j(2\omega_c t+\omega_r t+\frac{\pi}{2}+\phi+\theta_1-\theta_5)} \\ +\cos^2\theta e^{j(2\omega_c t+\omega_r t+\frac{3\pi}{2}+\theta_2-\theta_6)} \\ +\cos\theta\sin\theta e^{j(2\omega_c t+\omega_r t+\frac{3\pi}{2}+\phi+\theta_2-\theta_6)} \\ -\cos\theta\sin\theta e^{j(2\omega_c t+\omega_r t+\frac{3\pi}{2}-\phi+\theta_1-\theta_5)} \\ -\sin^2\theta e^{j(2\omega_c t+\omega_r t+\frac{\pi}{2}+\theta_1-\theta_5)} \\ +\cos\theta\sin\theta e^{j(2\omega_c t+\omega_r t+\frac{\pi}{2}-\phi+\theta_2-\theta_6)} \\ +\sin^2\theta e^{j(2\omega_c t+\omega_r t+\frac{\pi}{2}+\theta_2-\theta_6)} \end{Bmatrix} \quad (9)$$

By substituting (7) to (9) and we have

$$i_{PD-PolM} \propto (\sin(\tfrac{1}{2}z\ddot{\beta}(\omega_0)(2\omega_c\omega_r + {\omega^2}_r))\cos 2\theta - \sin 2\theta \sin\phi \cos(\tfrac{1}{2}z\ddot{\beta}(\omega_0)(2\omega_c\omega_r + {\omega^2}_r))) \quad (10)$$

The dispersive parameter can be expressed as [28]

$$D(\lambda_0) = \frac{(\omega_0)^2 z\ddot{\beta}(\omega_0)}{2\pi c} \quad (11)$$

By controlling the PC1, the phase difference can be adjusted to $\phi = \pi/2$, and substituting (11) to (10), the frequency response of the PolM-based scheme is obtained as

$$H(\omega_r)_{PolM} \propto \sin\left(2\theta - \frac{\pi c z D(\lambda_0)\omega_r(2\omega_c + \omega_r)}{(\omega_0)^2}\right) \quad (12)$$

According to Eq. (12), the frequency response of PolM -based DD scheme can be tuned by changing the angle of θ. In the conventional MZM-based DD scheme, the dual-color optical carrier is modulated by the same sinusoid RF signal with the angular frequency of ω_r as described in the PolM part, and the MZM is biased at quadrature point. The frequecny response of the conventional MZM-based scheme can be wirrten as

$$H(\omega_r)_{MZM} \propto \cos\left(\frac{\pi c z D(\lambda_0)\omega_r(2\omega_c + \omega_r)}{(\omega_0)^2}\right) \quad (13)$$

As shown in (13), the frequency response of conventional MZM-based scheme is fixed as the fiber length is unchanged.

According to the above-mentioned theoretical analysis, we have further investigated the frequency responses of both schemes in term of the experiment and simulation in the next section.

III. Experimental Set Up and Results of the Investigation on Frequency Response

To investigate above-mentioned frequency responses of both MZM-based and PolM-based DD schemes, we measure the electrical spectrum of the multi-tone signals after fiber transmission. The experimental setup is illustrated in Fig. 2(a) and the schematic diagrams of multi-tone signals show the expected results of both schemes. As the fiber length is fixed, the MZM-based scheme encounters fixed frequency notch at certain frequency. On the contrary, the proposed PolM-based scheme can manage the frequency notch by tuning its frequency response

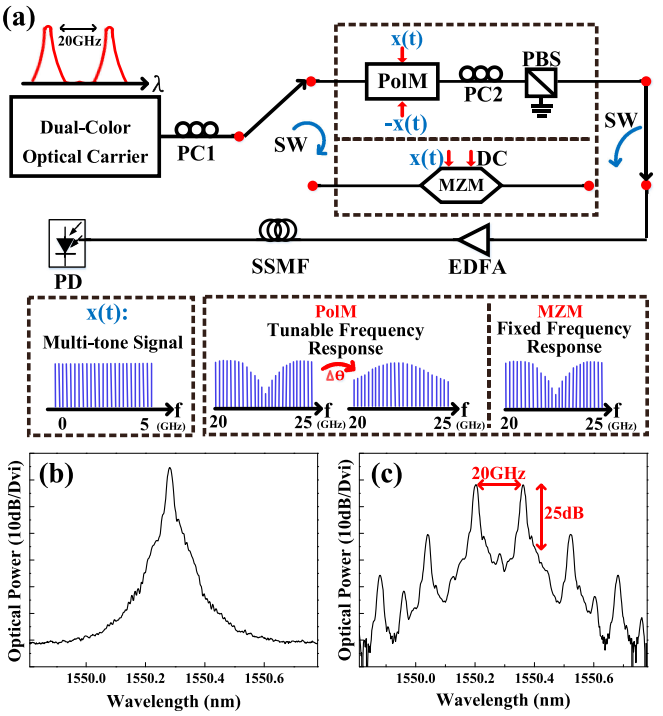

Fig. 2. (a) Experimental setup of both schemes. Measured optical spectra of the (b) tunable laser and (c) dual-color optical carrier. (EDFA: erbium-doped fiber amplifier.)

as changing the θvia PC2. In the dual-color optical carrier generation, a tunable laser emitted at 1550.28nm is launched to a 40-GHz MZM and modulated by a 10 GHz RF signal. The MZM is biased at its null point where the Vpi is 2.42V to generate the frequency doubling signal via carrier suppression. Fig. 2(b) and (c) show the measured optical spectra of the tunable laser and the dual-color optical carrier, respectively. Fig. 2(c) exhibits the dual-color optical carrier with 20 GHz wavelength spacing has achieved a high carrier suppression ratio of around 25 dB. Then the 200 multi-tone signals starting from 100 MHz to 5 GHz generated by the arbitrary waveform generator (AWG), with a sampling rate of 65 GSa/s and a bandwidth of 25 GHz, are launched to the PolM and MZM to modulate the dual-color optical carrier, respectively. In the PolM-based DD scheme, the modulated dual-color optical carrier is then passed to the PC2 prior to the PBS. After SSMF transmission, the PD converts the optical signals into the electrical signals which are captured by the real time oscilloscope (OSC) with a sampling rate of 80 GSa/s.

Fig. 3 shows the measured and simulated electrical spectra of the multi-tone signals after different SSMF transmissions as well as the simulated frequency responses. For the PolM-based scheme, the frequency notch is successfully shifted from 20 GHz to 25 GHz after 25-km SSMF by rotating the PC2 as shown in Fig. 3(a-1). The red curves stand for the simulated frequency response based on our theoretical model from Eq. (12). As the simulated frequency responses exhibit good matches with the experimental results, the corresponding θ to each frequency notches can be confirmed. To further verify the

Authorized licensed use limited to: Georgia Institute of Technology. Downloaded on July 08,2021 at 19:08:57 UTC from IEEE Xplore. Restrictions apply.

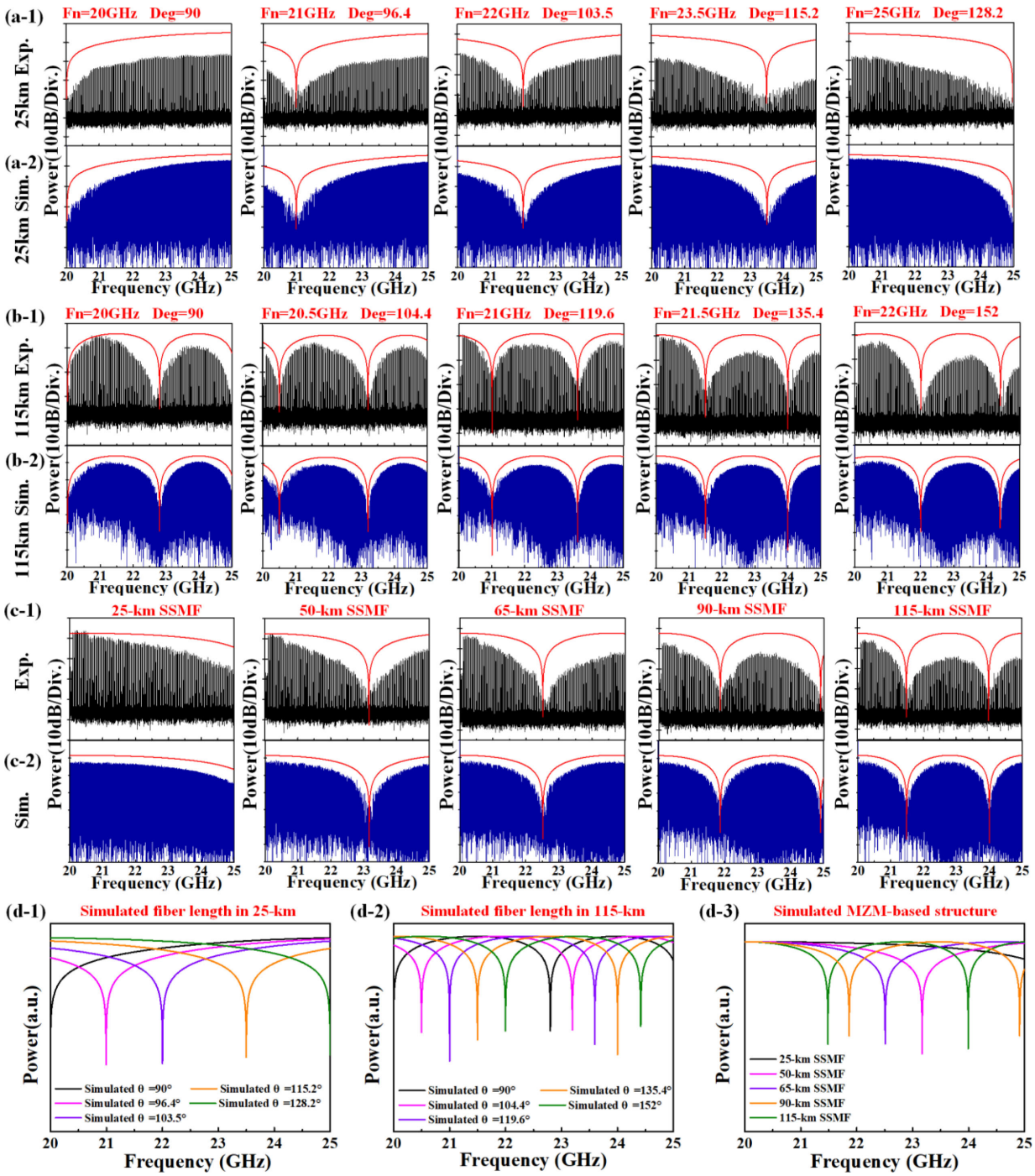

Fig. 3. Electrical spectra of the multi-tone signals by the proposed PolM-based scheme after 25-km SSMF transmission (via (a-1) experiment and (a-2) simulation) and 115-km SSMF transmission (via (b-1) experiment and (b-2) simulation). Electrical spectra of the multi-tone signals by the conventional MZM-based scheme after 25-km, 50-km, 65-km, 90-km, and 115-km SSMF transmission (via (c-1) experiment and (c-2) simulation). Simulated frequency responses of the proposed PolM-based scheme ((d-1):25km (d-2):115km) and (d-3) the conventional MZM-based scheme.

numerical model of the frequency response, we build a virtual experimental testbed in the simulation with the same parameters as the experimental setup. By designating the specific θ in the simulation, the simulated electrical spectra of multi-tone signals are obtained as shown in Fig. 3(a-2). The frequency notches of simulation results are located at the same frequencies as the experiment results, pointing that the experimental results and simulated frequency responses correlate with each other. Since the RF power fading effect becomes more severe when the fiber transmission distance is longer, a 115-km SSMF is employed and the measured and simulated electrical spectra are shown in Fig. 3(b-1) and (b-2), respectively. The first frequency notch appears at 20 GHz and it can be successfully shifted to 22 GHz by varying the θ from 90 to 152 degrees. Same as the

Authorized licensed use limited to: Georgia Institute of Technology. Downloaded on July 08,2021 at 19:08:57 UTC from IEEE Xplore. Restrictions apply.

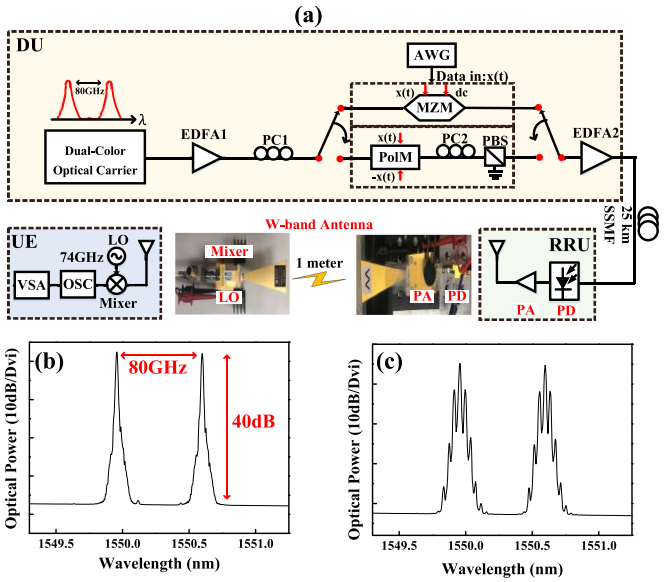

Fig. 4. (a) Experimental setup of the W-band RoF transport system of both schemes. Measured optical spectral of the dual-color optical carrier (b) before and (c) after modulation via PolM. (AWG: arbitrary waveform generator, UE: user equipment, LO: local oscillator, OSC: oscilloscope scope, VSA: vector signal analysis software.)

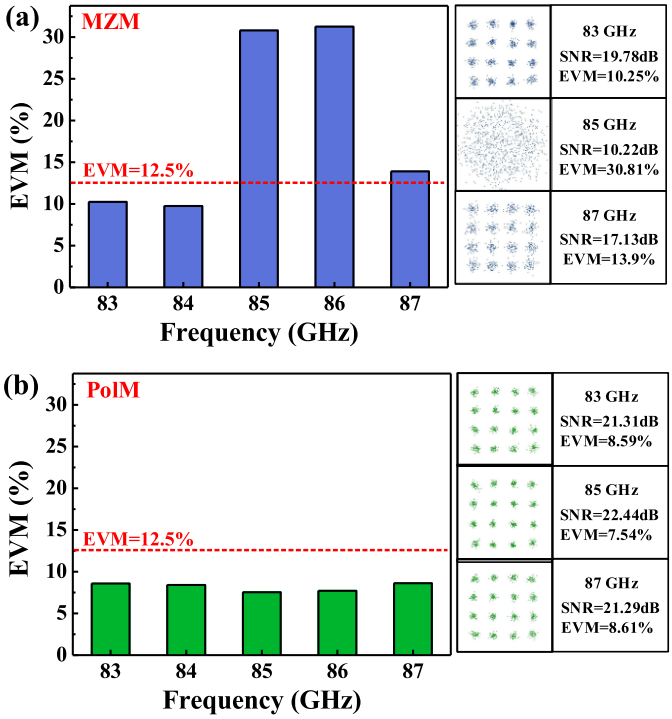

Fig. 5. Measured EVM, SNR and constellation diagrams from 83 GHz to 87 GHz of the (a) MZM-based DD scheme and (b) PolM-based DD scheme.

25-km SSMF, the experimental results agree with the theoretical analysis in the 115-km SSMF transmission. Additionally, the electrical spectra of the MZM-based DD scheme are also demonstrated in Fig. 3(c-1) and (c-2). Both the experimental and simulation results show that the frequency response only can be tuned by varying the fiber length and it is observed that the frequency notch is shifted to lower frequency as the fiber length is increased in the MZM-based scheme. To demonstrate the RF fading effect more straightforward, the simulated frequency responses for both schemes are illustrated in Fig. 3(d-1), (d-2) and (d-3). Since the operation bandwidth of the OSC is 25 GHz, the simulation only presents the frequency response from 20 to 25 GHz to fit the experiment results. Fig. 3(d-1) and (d-2) show the simulated frequency responses versus different $\theta$of 25- and 115-km SSMF in the PolM-based DD scheme, respectively. The second frequency notch is observed when the length of fiber is increased from 25 to 115 km and it also can be tuned flexibly by different θ. On the contrary, the frequency notch of the MZM-based DD scheme is fixed unless the fiber length is changed as shown in Fig. 3(d-3).

IV. Experimental Set Up and Results of the W-Band Transport System

The experimental setup of the W-band RoF transport system is shown in Fig. 4(a). We employed and operated the same tunable laser presented in section III at the DU side. The dual-color optical carrier with 80-GHz wavelength spacing is successfully generated by inserting a 40-GHz sinusoid signal to the MZM under its carrier suppress mode. A 50/100 GHz interleaver (IL) is utilized to increase the central carrier suppression ratio which is around 40 dB as shown in Fig. 4(b). The optical power of the dual-color optical carrier is boosted by an EDFA with 13.7-dBm output power. Then, the dual-color optical carrier is modulated by 16-QAM signals with different IF frequencies from 3 to 7 GHz with an increment of 1 GHz via MZM and PolM, respectively. Fig. 4 (c) shows the optical spectrum of the dual-color optical carrier after modulated by a 5 GHz 1Gbaud 16-QAM signal in the PolM-based scheme. The 1Gbaud 16-QAM signal is shaped by a root-raised cosine filter with the roll factor of 0.35 before the AWG output. Another EDFA is utilized to increase the optical power before the DU output. The 16-QAM signal is up-converted to W-band frequency from 83 GHz to 87 GHz via direct detection by a PD after transmitted by a 25-km SSMF. Then, the wireless data is delivered by a 25-dBi gain horn antenna after amplified by a W-band PA with 35-dB gain, at the RRU. After 1-meter on-air transmission, a paired horn antenna receives the wireless signal which is then mixed by a 74-GHz LO to down-convert its frequency to the IF band starting from 9 GHz to 13 GHz. Subsequently, the IF band signal is recorded by the OSC. The performance of the received signal is then evaluated after analog-to-digital conversion in terms of its error vector magnitude (EVM) and constellation diagrams through the Keysight vector signal analysis (VSA) software.

Fig. 5(a) and (b) show the measured EVM, signal-to-nose ratio (SNR) and constellation diagrams of the 1Gbaud 16-QAM signal with -2dB received optical power (ROP) after 25-km SSMF and 1-meter on-air transmission via the conventional MZM-based and the proposed PolM-based DD schemes, respectively.

Fig. 5(a) shows the measured EVM of the MZM-based scheme is strongly correlated to the RF power fading and the

Authorized licensed use limited to: Georgia Institute of Technology. Downloaded on July 08,2021 at 19:08:57 UTC from IEEE Xplore. Restrictions apply.

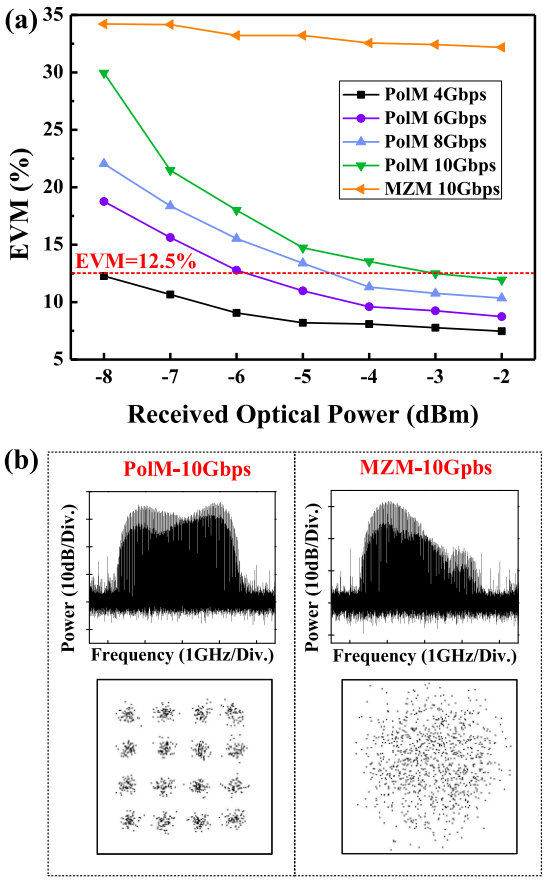

Fig. 6. (a) Measured EVM versus different ROPs of both schemes. (b) Measured electrical spectra and corresponding constellation diagrams of 10Gbps 16-QAM signal of both schemes.

EVM value of 85 GHz and 86 GHz is far from the 3rd Generation Partnership Project (3GPP) standard of 16-QAM signal (i.e. 12.5%). Therefore, this wastes the valued frequency resources in W-band due to the fixed frequency notches. In contrast to the MZM-based scheme, the measured EVM of the proposed scheme is relatively flat and with around 1.1% fluctuation within the frequency range from 83 GHz to 87 GHz. Moreover, the averaged EVM around 8.17% is achieved and the constellation diagrams of selected frequencies are also much clearer than those of the MZM-based DD scheme as shown on the right side of both Fig. 5(a) and (b). This can be understood that the RF fading can be circumvented by tuning the frequency notch far from the desired signals by varying θ via rotating the PC2. Different data rate of the 16-QAM signal located at 85 GHz are applied to both schemes to increase the transmission capacity. Fig. 6(a) illustrates the measured EVM performance of the 16-QAM signal with different data rate from 4 to 10 Gpbs versus different ROPs after 25-km SSMF and 1-meter wireless transmission. 10 Gbps is achieved at the ROP of -2 dBm under the specified 3GPP requirement in the PolM-based scheme. However, the signal cannot be restored even with only 1-Gbaud rate in the MZM-based scheme. Fig. 6(b) shows the electrical spectra of the down-converted 10Gpbs 16-QAM signals of both schemes. Due to the unavoidable frequency notch, the signal is severely degraded with a blurred constellation diagram in the MZM-based DD scheme whereas it can be recognized clearly in our proposed scheme.

V. Conclusion

We propose an RoF system based on a dual-color optical carrier generator using a polarization modulator with the capability of tunable frequency response in W-band. Detailed theoretical analysis of both proposed PolM-based and conventional MZM-based DD schemes are presented. To demonstrate desirable frequency responses of the dual-color optical carrier after different fiber transmission distances, the electrical spectra of the multi-tone signals are measured and validated. The measured electrical spectra are consistent with the simulated frequency responses, which prove the numerical analysis of theoretical models for both schemes is correct. In our W-band transport experiments, the PolM-based DD scheme, with tunable frequency response, successfully demonstrates stable system performance of transmitted 16-QAM signals from 83 GHz to 87 GHz with the averaged EVM value of 8.17% via 25-km SSMF and 1-m wireless transmission. For comparison, the conventional MZM-based DD scheme suffers from forbidden operation bands with frequency notches at 85 GHz and 86 GHz resulting in severe signal degradation. Furthermore, 10-Gbps 16-QAM signal located at 85 GHz is successfully transmitted by the proposed PolM-based DD scheme to deliver 10-gigabit signal over 25km SSMF in mobile fronthaul.

References

[1] L. R. Chen, "Chirped microwave and millimeter wave pulse generation based on optical spectral shaping and wavelength-to-time mapping in silicon photonics," *Opt. Commun., Special Issue Integr. Microw. Photon.*, vol. 373, pp. 70–81, 2016.

[2] L. R. Chen, P. Moslemi, Z. Wang, M. Ma, and R. Adams, "Integrated microwave photonics for spectral analysis, waveform generation, and filtering," *IEEE Photon. Technol. Lett.*, vol. 30, no. 21, pp. 1838–1841, Nov. 2018.

[3] G. K. Chang *et al.*, "Key new fiber wireless access technologies for 5G and beyond," *IEEE Future Netw. Tech Focus*, vol. 3, no. 2 Sep. 2019.

[4] J. Zhang *et al.*, "Enabling technologies for millimeter-wave radio-over-fiber systems in next generation heterogeneous mobile access networks," *Proc. SPIE*, vol. 10128, 2017, Art. no. 101280A.

[5] G. K. Chang and P. C. Peng, "Grand challenges of fiber wireless convergence for 5G mobile data communications [Invited]," in *Proc. Opto-Electron. Commun. Conf.*, Jul. 2018, pp. 1–2.

[6] C. H. Yeh *et al.*, "Utilizing single lightwave for delivering baseband/FSO/MMW traffics simultaneously in PON architecture," *IEEE Access*, vol. 7, pp. 138927–138931, 2019.

[7] H. Y. Wang, C. H. Cheng, C. T. Tsai, Y. C. Chi, and G. R. Lin, "28-GHz wireless carrier heterodyned from orthogonally polarized tri-color laser diode for fading-free long-reach MMWoF," *J. Lightw. Technol.*, vol. 37, no. 13, pp. 3388–3400, Jul. 2019.

[8] Z. K. Weng *et al.*, "Quasi-color-free LD-based long-reach 28-GHz MM-WoF With 512-QAM OFDM," *J. Lightw. Technol.*, vol. 36, no. 19, pp. 4282–4297, Oct. 1, 2018.

[9] C. Lim *et al.*, "Evolution of radio-over-fiber technology," *J. Lightw. Technol.*, vol. 37, no. 6, pp. 1647–1656, Mar. 2019.

[10] Y. Tong *et al.*, "Integrated silicon Photonics remote radio frontend (RRF) for single-sideband (SSB) millimeter-wave radio-over-fiber (ROF) systems," *IEEE Photon. J.*, vol. 11, no. 2, Apr. 2019, Art. no. 7202108.

[11] R. K. Shiu *et al.*, "A simplified radio-over-fiber system for over 100-km long-reach n-QAM transmission," *IEEE Photon. J.*, vol. 12, no. 3, Jan. 2020, Art. no. 7902908.

[12] S. Liu *et al.*, "A long-distance millimeter-wave RoF system with a low-cost directly modulated laser," *IEEE Photon. Technol. Lett.*, vol. 30, no. 15, pp. 1396–1399, Aug. 2018.

Authorized licensed use limited to: Georgia Institute of Technology. Downloaded on July 08,2021 at 19:08:57 UTC from IEEE Xplore. Restrictions apply.

[13] C. H. Chang *et al.*, "FTTH and two-band RoF transport systems based on an optical carrier and colorless wavelength separators," *IEEE Photon. J.*, vol. 8, no. 1, Dec. 2016, Art. no. 7900308.
[14] Y. C. Manie *et al.*, "Dual-output mach–zehnder modulator for optical access networks," *Fiber Integr. Opt.*, vol. 37, pp. 256–263, 2018.
[15] M. A. Bitew *et al.*, "Simultaneous transmission of wired and wireless signals based on double sideband carrier suppression," *Opt. Fiber Technol.*, vol. 38, pp. 108–112, 2017.
[16] Y. Alfadhli *et al.*, "Real-time FPGA demonstration of hybrid bidirectional MMW and FSO fronthaul architecture," in *Proc. Opt. Fiber Commun. Conf. Exhib.*, 2019, pp. 1–3.
[17] X. Li, J. Yu, J. Xiao, N. Chi, and Y. Xu, "W-band PDM-QPSK vector signal generation by MZM-based photonic frequency octupling and precoding," *IEEE Photon. J.*, vol. 7, no. 4, Aug. 2015, Art. no. 7101906.
[18] X. Li *et al.*, "Mm-wave vector signal generation and transport for W-band MIMO system with intensity modulation and direct detection," in *Proc. Conf. Opt. Fiber Commun.*, 2016, pp. 1–3.
[19] X. Li *et al.*, "W-band 8QAM vector signal generation by MZM-based photonic frequency octupling," *IEEE Photon. Technol. Lett.*, vol. 27, no. 12, pp. 1257–1260, Mar. 2015.
[20] H. T. Huang *et al.*, "High spectral efficient W-band OFDM-RoF system with direct-detection by two cascaded singledrive MZMs," *Opt. Express*, vol. 21, no. 14, pp. 16615–16620, 2013.
[21] Y. Y. Won, H. S. Kim, Y. H. Son, Y. H. Son, and S. K. Han, "Full colorless WDM-radio over fiber access network supporting simultaneous transmission of millimeter-wave band and baseband gigabit signals by sideband routing," *J. Lightw. Technol.*, vol. 28, no. 16, pp. 2213–2218, Aug. 2010.
[22] C. W. Chow, C. H. Yeh, M. G. Stanley, C. Li, and H. K. Tsang, "Long-reach radio-over-fiber signal distribution using single-sideband signal generated by a silicon-modulator," *Opt. Express*, vol. 19, no. 12, pp. 11 312–11 317, 2011.
[23] C. W. Chow, C. H. Yeh, and J. Y. Sung, "OFDM RF power-fading circumvention for longreach WDM-PON," *Opt. Express*, vol. 22, no. 20, pp. 24392–24397, Sep. 2014.
[24] X. Zou and J. Yao, "Repetition-rate-tunable return-to-zero and carrier-suppressed return-to-zero optical pulse train generation using a polarization modulator," *Opt. Lett.*, vol. 34, no. 3, pp. 313–315, 2009.
[25] S. Liu *et al.*, "Bandwidth-enhanced PAM-4 transmissions using polarization modulation and direct detection with a tunable frequency range," *J. Lightw. Technol.*, vol. 37, no. 3, pp. 1014–1022, Feb. 2019.
[26] R. K. Shiu *et al.*, "Tunable microwave photonic filter for millimeter-wave mobile fronthaul systems," in *Proc. IEEE Photon. Conf.*, 2018, pp. 1–2.
[27] R. K. Shiu *et al.*, "RF fading circumvention using a polarization modulator for supporting W-band RoF transport from 85 to 95 GHz," in *Proc. Opt. Fiber Commun. Conf. Exhib.*, 2020, pp. 1–3.
[28] R. K. Shiu *et al.*, "Performance enhancement of optical comb based microwave photonic filter by machine learning technique," *J. Lightw. Technol.*, to be published, doi: 10.1109/JLT.2020.2989210.

Run-Kai Shiu received the Ph.D. degree from the Department of Electro-Optical Engineering, National Taipei University of Technology, Taiwan, in 2020. From April 2019 to March 2020, he was a Visiting Researcher at the School of Electrical and Computer Engineering, Georgia Institute of Technology, Atlanta, U.S. His research interests include optical communication systems, fiber-wireless access technologies, and microwave photonics.

You-Wei Chen received the Ph.D. degree from the Institute of Photonics Technologies, National Tsing Hua University, Hsinchu, Taiwan, in 2016. He is now a Research Engineer and a Lab Manager at the School of Electrical and Computer Engineering, Georgia Institute of Technology, Atlanta, U.S. His research interests include wavelength division multiplexing, fiber-wireless integration networks (FiWIN), 6G radio access network (RAN) architecture, multi-access edge computing (MEC), all-spectra function decoupling network, beamforming system, and advanced waveforms.

Peng-Chun Peng received the Ph.D. degree from the Institute of Electro-Optical Engineering, National Chiao Tung University, Taiwan, in 2005. He is the Full Professor with the Department of Electro-Optical Engineering, National Taipei University of Technology. His research interests include fiber-wireless access technologies, optical communication systems, machine learning, and sensors. He has authored more than 120 SCI-ranked papers and nine granted U.S. patents. His publications have been cited over 2700 times (H-index: 26). He was invited as the technical program committee of Asia Communications and Photonics Conference (ACP), OptoElectronics and Communications Conference (OECC), International Topical Meeting on Microwave Photonics (MWP), and Optical Fiber Communication Conference (OFC).

Ming-Han Wen received the B.S. degree from the Department of Electronic Engineering from the National Yunlin University of Science and Technology, Taiwan, in 2019. He is currently pursuing the M.S. degree at the National Taipei University of Technology, Taiwan. His research interests include optical communication systems, fiber-wireless access technologies, and microwave photonics.

Shang-Jen Su received the M.S. degree from the Georgia Institute of Technology, GA, USA, in 2019. He is currently pursuing the Ph.D. degree in electrical engineering with the Georgia Institute of Technology, Atlanta, Georgia, USA. His research interests include radio-over-fiber and beamforming techniques in optical communication systems.

Chin-Wei Hsu was born in 1990. He received the Ph.D. degree from the Department of Photonics, National Chiao-Tung University, Hsinchu, Taiwan, in 2017. He is currently a Postdoctoral Researcher at the School of Electrical and Computer Engineering, Georgia Institute of Technology, Atlanta, U.S. His research interests include indoor positioning, visible light communication (VLC), fiber-wireless integration networks, and millimeter-wave (MMW) radio-over-fiber systems.

Gee-Kung Chang is the Georgia Research Alliance and Byers Eminent Scholar Chair Professor in Optical Networking at the School of Electrical and computer Engineering of Georgia Institute of Technology. He is currently the Director of the NSF Industry/University Cooperative Research Center for Fiber-Wireless Integration and Networking (FiWIN) for Hetergeneous Mobile Data Communications. He received the B.S. degree in physics from the National Tsing Hua University in Taiwan and the Ph.D. degree from the University of California, Riverside. Before joining Georgia Tech, Dr. Chang devoted 23 years of services in R&D at the Bell Labs, Bellcore, and Telcordia Technologies, where he served in various research and management positions including Director and Chief Scientist of Optical Internet Research. Prior to joining Georgia Tech he served as as the Vice President and Chief Technology Strategist of OpNext, where he was responsible for developing high speed integrated photonics devices and optical networking systems. Prof. Chang has coauthored more than 600 papers on peer-reviewed professional journals and international conferences. He is a fellow of both IEEE and OSA.

Authorized licensed use limited to: Georgia Institute of Technology. Downloaded on July 08,2021 at 19:08:57 UTC from IEEE Xplore. Restrictions apply.